Downloaded from orbit.dtu.dk on: May 05, 2023

DTU Library

The use of dynamic nuclear polarization (13)C-pyruvate MRS in cancer

Gutte, Henrik; Hansen, Adam Espe; Johannesen, Helle Hjorth; Clemmensen, Andreas Ettrup; Ardenkjær-Larsen, Jan Henrik; Nielsen, Carsten Haagen; Kjær, Andreas

Published in:
American Journal of Nuclear Medicine and Molecular Imaging

Publication date:
2015

Document Version
Publisher's PDF, also known as Version of record

Link back to DTU Orbit

Citation (APA):
Gutte, H., Hansen, A. E., Johannesen, H. H., Clemmensen, A. E., Ardenkjær-Larsen, J. H., Nielsen, C. H., & Kjær, A. (2015). The use of dynamic nuclear polarization (13)C-pyruvate MRS in cancer. *American Journal of Nuclear Medicine and Molecular Imaging*, *5*(5), 548-60.

General rights
Copyright and moral rights for the publications made accessible in the public portal are retained by the authors and/or other copyright owners and it is a condition of accessing publications that users recognise and abide by the legal requirements associated with these rights.

- Users may download and print one copy of any publication from the public portal for the purpose of private study or research.
- You may not further distribute the material or use it for any profit-making activity or commercial gain
- You may freely distribute the URL identifying the publication in the public portal

If you believe that this document breaches copyright please contact us providing details, and we will remove access to the work immediately and investigate your claim.

Am J Nucl Med Mol Imaging 2015;5(5):548-560
www.ajnmmi.us /ISSN:2160-8407/ajnmmi0010834

Review Article

The use of dynamic nuclear polarization ^{13}C-pyruvate MRS in cancer

Henrik Gutte[1], Adam Espe Hansen[1], Helle Hjorth Johannesen[1], Andreas Ettrup Clemmensen[1], Jan Henrik Ardenkjær-Larsen[2,3,4], Carsten Haagen Nielsen[1], Andreas Kjær[1]

[1]Department of Clinical Physiology, Nuclear Medicine & PET and Cluster for Molecular Imaging, Rigshospitalet and University of Copenhagen, Denmark; [2]Danish Research Centre for Magnetic Resonance, Centre for Functional and Diagnostic Imaging and Research, Copenhagen University Hospital Hvidovre, Denmark; [3]Department of Electrical Engineering, Technical University of Denmark, Kgs Lyngby, Denmark; [4]GE Healthcare, Brøndby, Denmark

Received May 29, 2015; Accepted July 31, 2015; Epub October 12, 2015; Published October 15, 2015

Abstract: In recent years there has been an immense development of new targeted anti-cancer drugs. For practicing precision medicine, a sensitive method imaging for non-invasive, assessment of early treatment response and for assisting in developing new drugs is warranted. Magnetic Resonance Spectroscopy (MRS) is a potent technique for non-invasive *in vivo* investigation of tissue chemistry and cellular metabolism. Hyperpolarization by Dynamic Nuclear Polarization (DNP) is capable of creating solutions of molecules with polarized nuclear spins in a range of biological molecules and has enabled the real-time investigation of *in vivo* metabolism. The development of this new method has been demonstrated to enhance the nuclear polarization more than 10,000-fold, thereby significantly increasing the sensitivity of the MRS with a spatial resolution to the millimeters and a temporal resolution at the subsecond range. Furthermore, the method enables measuring kinetics of conversion of substrates into cell metabolites and can be integrated with anatomical proton magnetic resonance imaging (MRI). Many nuclei and substrates have been hyperpolarized using the DNP method. Currently, the most widely used compound is ^{13}C-pyruvate due to favoring technicalities. Intravenous injection of the hyperpolarized ^{13}C-pyruvate results in appearance of ^{13}C-lactate, ^{13}C-alanine and ^{13}C-bicarbonate resonance peaks depending on the tissue, disease and the metabolic state probed. In cancer, the lactate level is increased due to increased glycolysis. The use of DNP enhanced ^{13}C-pyruvate has in preclinical studies shown to be a sensitive method for detecting cancer and for assessment of early treatment response in a variety of cancers. Recently, a first-in-man 31-patient study was conducted with the primary objective to assess the safety of hyperpolarized ^{13}C-pyruvate in healthy subjects and prostate cancer patients. The study showed an elevated ^{13}C-lactate/^{13}C-pyruvate ratio in regions of biopsy-proven prostate cancer compared to non-cancerous tissue. However, more studies are needed in order to establish use of hyperpolarized ^{13}C MRS imaging of cancer.

Keywords: Dynamic nuclear polarization, cancer, ^{13}C-pyruvate, MR, MRS, response monitoring

Introduction

Increasingly, therapies are tailored either through targeting specific abnormalities, e.g. genetic mutations, or through early response monitoring. Sensitive methods for non-invasive *in vivo* imaging assessment of early treatment response as well as assisting in developing new drugs are warranted. Positron Emission Tomography (PET) imaging with fluorodeoxyglucose (FDG) has been established as a clinical tool in molecular imaging. FDG is a glucose analog labeled with the positron-emitting isotope ^{18}F. It is transported across the cell membrane by glucose transporters (GLUTs), phosphorylated by hexokinase, trapped in the cell and accumulates in proportion to local metabolism. Increased ^{18}F-FDG uptake is then detected using a PET scanner [1]. ^{18}F-FDG uptake can be measured using standardized uptake value (SUV), which is a quantitative measure of radioactivity concentration in PET images normalized to injected dose and body weight, ^{18}F-FDG SUV thus measures tumor metabolic activity. However, this standard has certain limitations and can be affected by factors such as blood glucose level in the patient [2]. Conventional computed tomography (CT) is a sensitive ana-

Table 1. Table with MR biologically interesting nuclides and demonstrating, that only the nuclei of phosphor (^{31}P) and hydrogen (^{1}H) exist in high enough concentrations to be used for routine clinical evaluation [70]

Nuclide	Abundance in tissue	MR-detect. isotope	Abundance of isotope	Abundance in tissue
H	63%	^{1}H	99.99%	63%
C	12%	^{13}C	1.1%	0.13%
N	0.58 %	^{15}N	0.37%	0.0021%
O	24%	^{17}O	0.038%	0.0091%
P	0.22%	^{31}P	100%	0.22%

tomical scanning technique in tumor imaging, however it lacks physiological information. Introduction of new CT techniques (dual energy CT and CT perfusion imaging with iodine contrast agents) together with recent advances in hardware has improved spatial and temporal resolution, and physiological information is now obtainable from CT datasets. Nevertheless, when evaluating treatment response, consecutive acquisitions are usually performed yielding a substantial radiation burden; therefore non-ionizing methods should be considered as an alternative. Diffusion Weighted Magnetic Resonance Imaging (DW-MRI) is non-ionizing and measures the movement of proton nuclei, primarily from water, and thereby demonstrates tissue cellularity and integrity of cell membranes. Diffusion based MRI has proven to be useful for staging and predicting prognosis of cancer patients. However, diffusion based MRI is only sensitive to structural information and lacks metabolic information [3].

MR spectroscopy

Magnetic Resonance Spectroscopy (MRS) imaging is like MRI based on the principle of nuclear magnetic resonance (NMR). MRS is a potent technique for non-invasive *in vivo* investigation of tissue chemistry. MRS has been widely applied in biochemistry research for the analysis of basic organic compounds and provides information about e.g. tissue metabolites. Conventional proton MRI uses magnetic gradients to create controlled perturbations of the magnetic field, thus creating anatomical images. MRS likewise codes the spatial dimensions, but in addition, utilizes the miniscule differences in resonance frequency of the various nuclei, depending on the molecular structure, creating an accurate illustration of metabolic chemistry *in situ*. In theory, many biochemically relevant nuclides, such as hydrogen (^{1}H), carbon (^{13}C), nitrogen (^{15}N), fluorine (^{19}F), sodium (^{23}Na) and phosphor (^{31}P) possess a magnetic moment and can be used for MRS. However, only the nuclei of phosphor (^{31}P) and hydrogen (^{1}H) exist in high enough concentrations to be used for routine clinical evaluation, see **Table 1**. Depending on the chemical structure of the molecule, the nuclei responsible for the NMR signal is exposed to a slightly different magnetic environment, hence resonating at a slightly different frequency. This way various metabolites can be quantified. The method is primarily used in brain and prostate cancer and spectra associated with tumor tissue are distinguished from those associated with normal tissue by the characteristic increase in the resonance peak of choline corresponding to increased cell membrane density [4, 5]. There are several limitations to this technique, with consequential decrease of temporal resolution to the minute scale and of spatial resolution to 1 cm^3 depending on the nucleus detected and of the magnetic field strength [6, 7]. Moreover, spectroscopic images of tissue metabolites lack dynamic information about metabolic fluxes [8].

Dynamic nuclear hyperpolarization

A more sensitive method that allows real time imaging of the dynamics of the metabolism is therefore necessary. Hyperpolarization in the context of NMR refers to the process of relocating the nuclei temporarily into a redistribution of energy levels [9]. The hyperpolarization process can be accomplished by a number of techniques; 1) optical pumping, which is primarily in use for noble gases as ^{3}He and ^{129}Xe in lung perfusion imaging [10], 2) PHIP (para hydrogen-induced polarization) which suffers from the limited number of metabolic substrates that can be hyperpolarized [11, 12] or 3) dynamic nuclear hyperpolarization (DNP). A more extensive description of the two former methods can be found elsewhere and is beyond the scope of this paper.

Ardenkjaer-Larsen et al. first described hyperpolarization with DNP and was established on DNP in the solid state. The method is based on the development of a dissolution technique

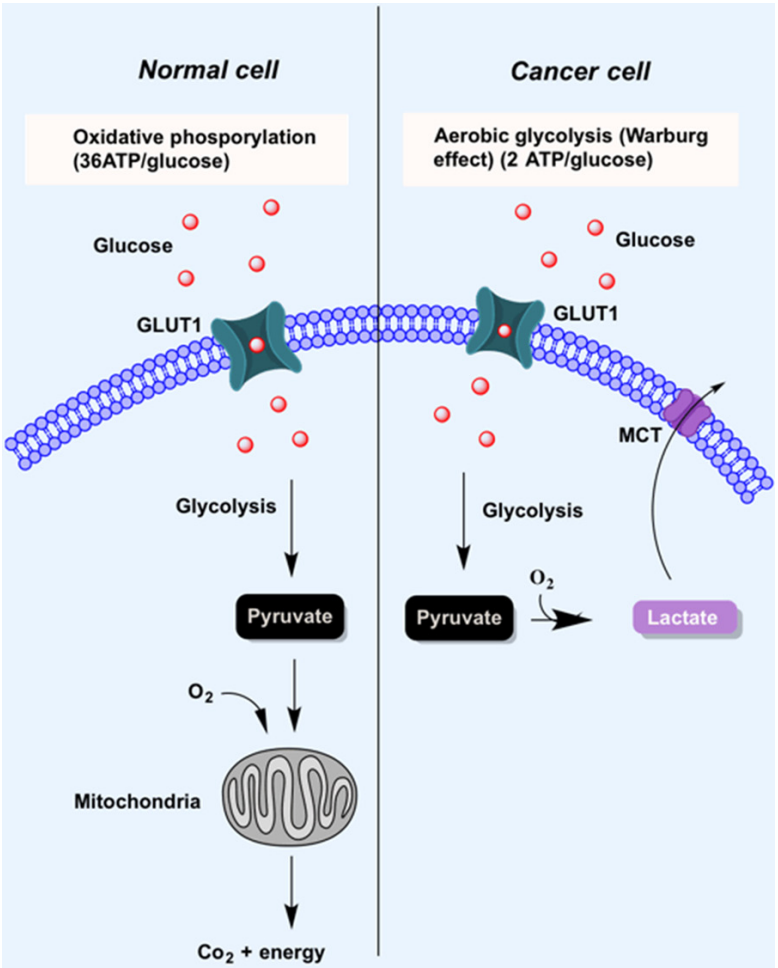

Figure 1. A key metabolic fingerprint in cancer cells is the switch to glycolysis with production of lactate even in the presence of sufficient oxygen (reproduced with permission from ref [68]).

that preserves the nuclear polarization during the transition from solid to liquid state. The method is capable of creating solutions of molecules with polarized nuclear spins in various molecules and has enabled the real-time investigation of *in vivo* metabolism [13, 14]. The procedure consists of polarization transfer from electrons to nuclei in solids by microwave irradiation. The solution to be polarized typically contains ^{13}C-enriched substrates; a free stable radical is dissolved in a glass-forming solvent and then positioned into a high magnetic field (e.g. 3 T). The free radical provides unpaired electrons and the glassing material optimize the efficiency of microwave energy transfer. The compound is brought to very low temperature (≈1 K) and irradiated. After the polarization transfer, the microwaves are turned off, and the metabolite is warmed rapidly to room temperature with substantial retention of the polarization that was present in the frozen solid state. It is then quickly transferred and injected into the specimen or animal for MRI acquisition. The nuclear spin polarization is proportional to gamma (γ) and B_0/T where γ is the nucleus specific gyromagnetic ratio constant, B_0 is the applied magnetic field and T is temperature. With this method, a liquid state polarization of up to 64% has been achieved [15]. The time for the polarization to build up to maximum level is about one hour.

The use of this new method has enhanced the nuclear polarization more than 10,000-fold. It has resulted in a significantly increased sensitivity of the MRS and increased the spatial resolution to the millimeter scale and the temporal resolution to the sub second range. Furthermore, these advances makes it possible to measure the kinetics of the conversion of the metabolite into other cell metabolites and can be integrated with anatomic proton MRI [14]. One limitation, however, is a relatively short half-life (10-30 s in vivo) of the hyperpolarized metabolites. Therefore, the solution requires rapid transfer into the patient and the imaging sequence must be efficient and accomplished within 2-3 minutes and the metabolites must be metabolized and transferred across the cell membrane very rapidly [14].

Many nuclei have been hyperpolarized using the DNP method. Currently, the most widely used metabolite is ^{13}C-pyruvate due to the optimal gyromagnetic ratio, the relatively long relaxation time and finally the possibility of incorporating ^{13}C into biological relevant metabolites [16, 17]. Intravenous injection of the hyperpolarized ^{13}C-pyruvate results in an increase of ^{13}C-lactate, ^{13}C-alanine and ^{13}C-

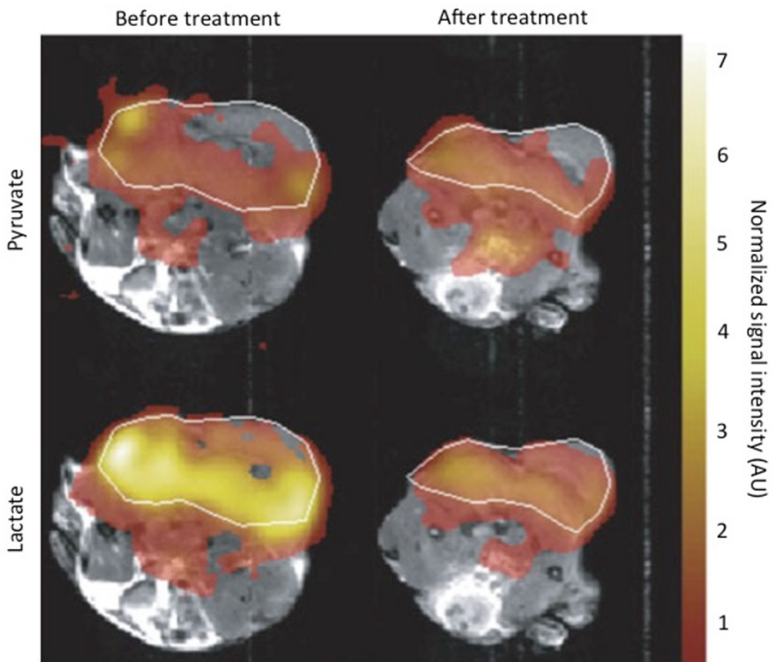

Figure 2. Color maps representing ^{13}C-lactate and ^{13}C-pyruvate peak intensities obtained from ^{13}C chemical-shift images in the same mouse before and after treatment with etoposide. The images were acquired between 20 and 25 s after intravenous injection of 0.2 ml 75 mM hyperpolarized ^{13}C-pyruvate and 20 h after injection of the mice with 67 mg/kg etoposide. Tumor margins are indicated by the white lines. Reprinted with kind permission from Nature Medicine [30].

bicarbonate resonance peaks depending on the tissue, disease and the metabolic state probed. In cancer, ^{13}C-lactate is increased due to increased glycolysis. Numerous studies have shown that glycolysis and production of lactate and alanine is increased in tumor cells compared to normal cells even when oxygen is sufficient a phenomenon known as Warburg effect [18], as shown in **Figure 1**.

Use of hyperpolarized ^{13}C-pyruvate in cancer

Detecting tumor response to treatment

Currently treatment response is assessed by imaging measurement to monitor anatomical tumor reductions in accordance with the latest guidelines of the "Response Evaluation Criteria In Solid Tumors" (RECIST). Here, partial response to treatment is defined as "at least a 30% decrease in the sum of the longest diameter of target lesions, taking as reference the baseline sum longest diameter" [19]. However these anatomic changes defining partial response may take weeks to develop in tumors and in some cases not develop at all or even demonstrate growth due to tumor stasis after treatment [20, 21]. In these situations ineffective treatment or even harmful treatment can be given. Consequently, ^{18}F-FDG-PET imaging has or is under investigation for therapy response assessment in many tumors. Quantitative estimation of ^{18}F-FDG uptake by SUV in tumor has demonstrated a distinct reduction of glucose to predict response of treatment, despite the fact that tumor increased in size [22]. However, ^{18}F-FDG-PET lacks sensitivity to certain tumor types, due to low ^{18}F-FDG uptake (e.g. prostate cancer) [23], high uptake in surrounding tissue (brain cancers) [24] or specificity due to ^{18}F-FDG uptake in infected or inflamed tissue [25]. In addition, high ^{18}F-FDG uptake of infiltrating immune cells after treatment can mask the decreased uptake by the dying cancer cells and correlates with the number of metabolically active viable cells, regardless of whether they are tumoral or non-tumoral in nature. Sustained high ^{18}F-FDG uptake can occur in a tumor mass after administration of chemotherapy due to infiltrating macrophages [26]. Lastly, PET exposes the patient to significant radiation burden and can only be repeated a limited number of times.

Proton based MRS has the potential to provide routine assessment of cancer treatment. However, it is still a relatively novel technology and more work is required to validate the biomarkers that MRS can detect [27]. In an orthotopic animal model of glioma, it was investigated whether changes in ^{1}H MRS metabolites could render reliable biomarkers for an early response to suberoylanilide hydroxamic acid (SAHA) treatment which blocks histone deacetylation activity and results in the accumulation of acetylated histones and proteins, such as transcription factors essential for expres-

sion of genes necessary to induce cell differentiation [28]. Wei et al. demonstrated a decrease in the concentration of lactate in tumors of treated rats. These results indicate that SAHA inhibits tumor growth and induces normal brain tissue-like metabolism in brain tumors [29]. One of the earliest studies using hyperpolarized ^{13}C-pyruvate in treatment response in cancer used lymphoma lesion in mice treated with topoisomirase inhibitor (Etoposide). Etoposide induces loss of NAD(H) and decrease in LDH activity and consequently apoptosis with demonstration of decreased flux in hyperpolarized ^{13}C-pyruvate and ^{13}C-lactate [30], see **Figure 2**. This flux is inhibited within 24 hours of treatment. Witney et al. compared ^{18}F-FDG-PET and hyperpolarized ^{13}C-pyruvate for detecting tumor response to treatment of murine lymphoma and demonstrated that the timing of response varied. The decreased ^{18}F-FDG uptake was preceded by the decrease in flux of ^{13}C metabolite between pyruvate and lactate, however with equal relative reductions in both ^{18}F-FDG and hyperpolarized ^{13}C-pyruvate/^{13}C-lactate. This suggests that the most important advantage of hyperpolarized MRI may be in response assessment in cancers where ^{18}F-FDG-PET is insensitive [31]. Decreased hyperpolarized ^{13}C-lactate was also shown in a cell line of human breast adenocarcinoma treated with another topoisomirase inhibitor (doxorubicin) where the level of hyperpolarized ^{13}C-lactate production was decreased before any detectable change in tumor size reflecting DNA [32]. The phosphatidylinositol 3-kinase (PI3K) pathway has been found to have key regulatory roles in many cellular processes, including cell survival, proliferation, glucose metabolism and cell differentiation. Several anti cancer therapeutic drugs targeting the pathway are in clinical trials [33]. Traditional imaging methods such as CT and MRI are inadequate in monitoring early treatment response due to tumor stasis rather than shrinkage associated with PI3K inhibition [34]. Hyperpolarized ^{13}C-pyruvate was used in mice with subcutaneously implanted glioblastoma xenografts detecting the effect of PI3K inhibition and produced a decrease of hyperpolarized ^{13}C-lactate. This finding was then confirmed in mice with breast cancer cells and associated with reduction in LDH activity of expression and hypoxia-inducible factor-1α proteins (HIF-1α) [35]. This was also shown in a more clinically relevant model involving invasive orthotopic (intracranial) glioblastoma xenografts in rats treated with Everolimus, an mTOR inhibitor that is part of the PI3K pathway [36]. The same mouse model was also treated with the most frequently used chemotherapeutic in treating glioblastoma, Temozlomide, an alkylating agent that works by damaging DNA. It was demonstrated that the ratio of hyperpolarized ^{13}C-pyruvate to ^{13}C-lactate was increased in the treatment group [37]. Cell signalling through the PI3K pathway can be inhibited by various receptor tyrosine kinase inhibitors (RTK) (Imatinib) and was associated with receptors for the stem cell factor (c-KIT) and platelet-derived growth factor (PDGFR) [38]. In a prostate cancer model inhibition of PDGFR with Imatinib reduced the flux of hyperpolarized ^{13}C-lactate by lowering the expression of LDH itself, which was mediated, by reduced expression of their transcriptional factors HIF-1α and c-MYC [39]. Vascular disrupting agents are chemotherapeutics that selectively targets endothelial cell and leads to tumor cell necrosis and is not triggering tumor shrinkage [40]. Vascular function has been measured using dynamic contrast agent-enhanced MRI and ^{15}O-H_2O-PET, however the necessity of a wide variety of kinetic models and an onsite cyclotron and has limited its use in clinical practice. In a murine lymphoma model, the rate of flux of hyperpolarized ^{13}C between pyruvate and lactate was decreased by 34% within 6 and 24 hours of treatment with the vascular disrupting agent combrestatin-A4-phosphate (CA4P). A simultaneously change on dynamic contrast agent-enhanced MRI after 6 hours was demonstrated, which was normal after 24 hours. DWI MR showed no change on the ADC (apparent diffusion coefficient) of tumor after 6 hours of treatment, although a decrease after 24 hours was observed and therefore it was concluded that hyperpolarized ^{13}C-pyruvate might provide a more sensitive indicator in vascular disrupting drugs than the traditionally used MR modalities [41]. The same group also demonstrated that hyperpolarized ^{13}C MRS can detect the early effects of anti-angiogenic therapy (bevacizumab, Avastin) in 2 colorectal cancer xenograft models (LoVo and HT29), which are known to display differential response to VEGF (vascular endothelial growth factor) blockade [42].

Other categories of treatment against cancer have also been examined. In the TRAMP model,

Table 2. Overview of studies investigating treatment of response of cancer with hyperpolarized ^{13}C-pyruvate

Therapy	Host	Cancer type	Cancer cell line	Tumor inoculation	13C-pyruvate/ lactate response	Other imaging modalities	Reference
Etoposide	Mice	Lymphoma	EL-4 (moue)	S.c.	Decreased ^{13}C-lactate		[30]
Etoposide	Mice	Lymphoma	EL-4 (mouse)	S.c.	Decreased ^{13}C-lactate	^{18}F-FDG-PET: Decreased SUV.	[31]
Doxyrubicin	Cell media	Breast adenocarcinoma	MDA-MB-231 (Human)		Decreased ^{13}C-lactate		[32]
LY294002	Cell media	Glioblastoma	GS-2 (human)		Decreased ^{13}C-lactate		[35]
Everolimus	Cell media	Breast adenocarcinoma	MDA-MB-231 (human)		Decreased ^{13}C-lactate		[35]
Everolimus	Mice	Glioblastoma	GS-2 (human)	S.c.	Decreased ^{13}C-lactate		[35]
Everolimus	Mice	Glioblastoma	GS-2 (human)	I.c.	Decreased ^{13}C-lactate	MRI (T2, T1GD): No response.	[36]
Imatinib	Mice	Prostate adenocarcinoma	PC-3MM2 (human)	Tibia	Decreased ^{13}C-lactate	MRI (DCE): Significant decease in vascular permeability.	[39]
Imatinib/ Paclitaxel	Mice	Prostate adenocarcinoma	PC-3MM2 (human)	Tibia	Decreased ^{13}C-lactate	MRI (DCE): Significant decease in vascular permeability.	[39]
Combretastatin-A4-phosphate	Mice	Lymphoma	EL-4 (mouse)	S.c.	Decreased ^{13}C-lactate	MRI (DCE): Significant suppression of uptake at 6 h after treatment, returning to above pretreatment values at 24 h. DWI: 6 h after treatment no change, 24 h after treatment increase in ADC.	[41]
Bevacizumab (Avastin)	Mice	Colorectal adenocarcinoma	LoVo (human)	S.c.	Decreased ^{13}C-lactate	MRI (DCE): Antivascular effects were observed at 24 h after the first dose of, but began to recover after the second dose (72 hours. DWI: No change in ADC).	[42]
Bevacizumab (Avastin)	Mice	Colorectal adenocarcinoma	HT29 (human)	S.c.	Increased ^{13}C-lactate	MRI (DCE): No antivascular effects. DWI: Decrease in ADC after 72 h of treatment.	[42]
Androgen deprivation	Mice	Prostate Adenocarcinoma	TRAMP	(orthotopic)	Decreased ^{13}C-lactate		[43]
Radiotherapy	Rats	Glioma	C6 (rat)	I.c.	Decreased ^{13}C-lactate		[44]

S.c.: subcutaneous. I.c.: intracranial. DCE: dynamic contrast enhancement.

anti-androgenic therapy demonstrated that hyperpolarized ^{13}C-pyruvate correlated with disease progression and increased in untreated animals [43]. In addition, the pre-treatment ^{13}C-lactate to ^{13}C-pyruvate ratio was a predictor of treatment outcome [2]. Day et al. investigated a rat model of gliobastoma in treatment of radiotherapy and ^{13}C hyperpolarization. It was demonstrated that a response could be detected after radiotherapy through decreased ^{13}C labeling of tumor lactate. Response could be detected even though an increase in tumor volume was demonstrated [44]. This study shows that it may be possible to distinguish between true progression and pseudo progression due to tumor stasis and could be used to guide subsequent treatment using hyperpolarized ^{13}C-pyruvate. An overview of treatment response studies is given in **Table 2**.

Application in brain tumor imaging

^{18}F-FDG-PET studies have shown increased rate of glucose uptake, increased expression of GLUT transporters in numerous cancers and a correlation of glucose uptake and accumulation of lactate with the aggressiveness and prognosis [45]. The application of ^{18}F-FDG-PET in clinical neuro-oncology is limited by the high background uptake of normal gray matter and low specificity [24]. Therefore other investigations are warranted in brain tumor imaging. Several studies have demonstrated that increased lactate production is found in human glioma [46] and rat glioma models [47]. Proton MRS (^{1}H MRS) has been one tool to characterize lactate production of brain tumors and elevated lactate has been associated with poor survival in patients with glioblastoma multiforme [48]. However the interpretation of MRS is difficult in this highly heterogeneous tumor, since increased lactate level is dependent upon increased glycolysis and rate of lactate production and clearance. Furthermore, because of the complexity in separating the lactate peaks from cystic and necrotic regions. Consequently an alternative technique for assessing the tumor metabolism is necessary. Park et al. compared the in-vivo metabolism in malignant glioma and normal rat brain with two different human glioma xenografts (U-251 MG and U-87) and demonstrated the feasibility of hyperpolarized ^{13}C-pyruvate in characterizing brain tumors from normal brain and between the different glioma cell lines [37, 49].

Application in prostate cancer imaging

Prostate cancer is the second leading cause of cancer deaths in men. Most men diagnosed at a very early stage will die with prostate cancer but not from the disease [50]. Distinguishing lethal from clinically indolent disease is a paramount interest in prostate cancer management. So far prostate cancer is diagnosed by histopathologic samples from the gland by random transrectal biopsies. Gleason grading on histopathological examination is the best prognostic indicator in prostate cancer to date; though, grading on biopsies may not correlate with the prostatectomy specimen because of sampling errors, interobserver variation, and morphologically identical prostate cancer can behave differently [51]. The transgenic adenocarcinoma of mouse prostate (TRAMP) model mimics that of human prostate cancer. The TRAMP model develops progressive, heterogeneous and multifocal disease and spontaneous prostatic neoplasia which progresses to carcinoma and metastasis in lymph nodes, lungs and less frequently liver, adrenal glands and bones [52]. The first study with hyperpolarized ^{13}C-pyruvate was applied in the TRAMP model by Chen et al. and presented the feasibility of detecting rapid cellular conversion of ^{13}C-pyruvate to ^{13}C-lactate in tumor and allowed the acquisition of 3D MRS in approximately 10 s with a spatial resolution of 0.135 cm^3 [53]. Serial data from Albers et al. demonstrated that it was possible to differentiate and measure the histological grade on the basis of ^{13}C-lactate levels in normal prostate, low-grade tumors and high-grade tumors. ^{13}C-lactate levels and histological grade had a correlation coefficient of 0.95. Additionally, lymph node metastasis had significantly elevated levels of ^{13}C-lactate as well [54]. Lupo et al. confirmed this and demonstrated that variations in ^{13}C-lactate signal intensities were apparent for different stages of disease development, with correlation between elevated ^{13}C-lactate levels and advanced disease. The intensity of the ^{13}C-lactate level varied spatially within the tumor consistent with the known heterogeneity of the disease [55]. To evaluate the use of hyperpolarized ^{13}C-pyruvate on a larger scale, Nelson et al. demonstrated the feasibility in healthy dogs because of the resemblance in

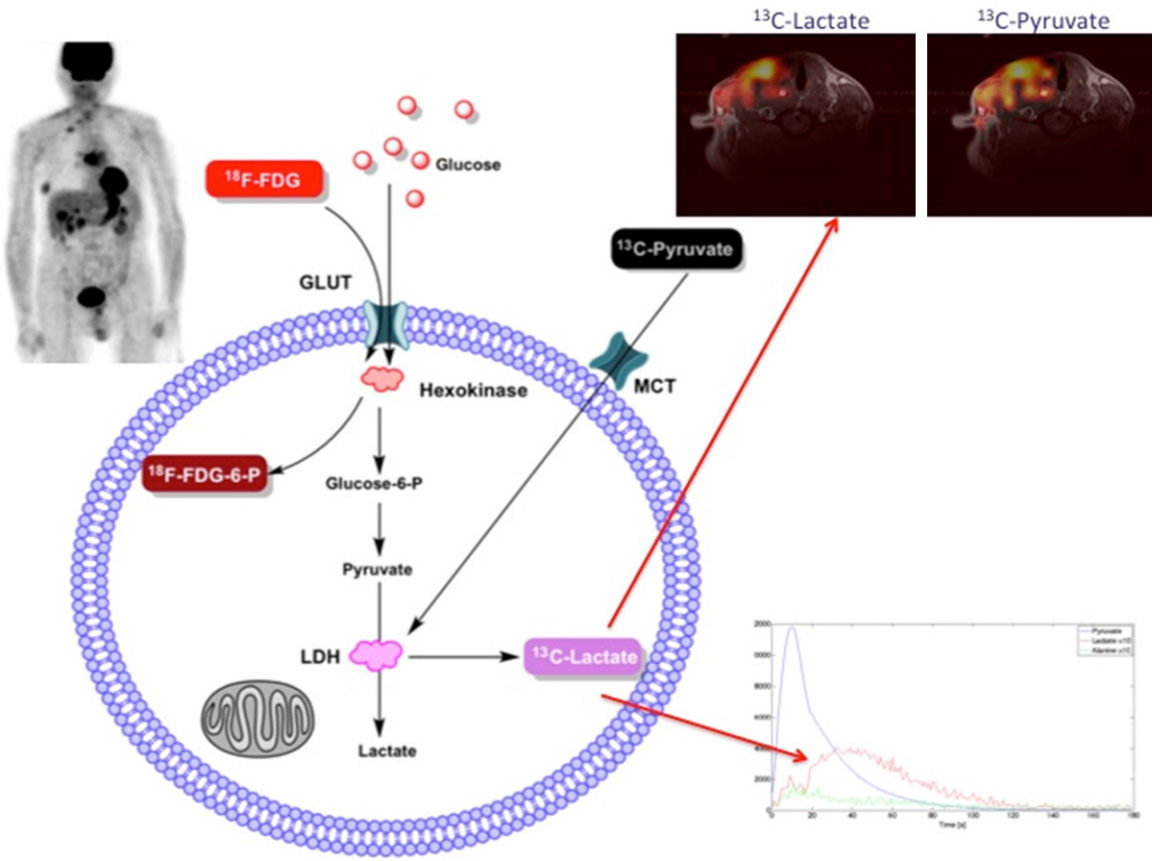

Figure 3. View of HyperPET and description of the *Warburg effect*. Increased ^{18}F-FDG uptake is a composite quantity of numerous hallmarks of cancer, *e.g.* metabolic changes, cell proliferation and hypoxia. While measured ^{13}C-pyruvate to ^{13}C-lactate switch probably expresses the Warburg *per se*. Modified from [68].

anatomy and size of the prostate gland to that of the human. Coil geometry, data acquisition parameters and radiofrequency pulses were developed and provided a realistic test of the methodology. The observed ^{13}C-lactate to ^{13}C-pyruvate ratio was significantly lower than previously seen in kidneys and tumors of smaller animals but was still increased in the healthy dog prostate [56].

A phase 1 "Ascending-dose study to assess the safety and tolerability and imaging potential of hyperpolarized pyruvate (^{13}C) injection in subjects with prostate cancer" was undertaken at the University of California, San Francisco. This first-in-man 31-patients study was conducted with the primary objective to assess the safety of hyperpolarized ^{13}C-pyruvate in healthy men and prostate cancer patients, and confirmed the safety of the agent. In addition it showed elevated ^{13}C-lactate/^{13}C-pyruvate ratio in regions of biopsy-proven prostate cancer compared to non-cancerous tissue of the prostate [57].

Application in breast cancer

The metabolite flux depends upon delivery of pyruvate via the vasculature, on the rate of pyruvate transport across the plasma cell membrane and on the concentration of lactate dehydrogenase (LDH) and its substrates. Consequently, understanding the changes in lactate levels will require interpreting the relative significance of these steps in establishing the kinetics of metabolite exchange [14]. In human breast cancer cells, it was shown that the flux of hyperpolarized ^{13}C-pyruvate assuming simple Michaelis-Menten kinetics was transferred to the cell as determined by the monocarboxylic acid transporter-1 (MCT). MCT is a member of a family of trans-membrane proteins, which introduces pyruvate into the glycolytic pathway. Conversely the addition of a

MCT1 inhibitor (Quercetin) markedly reduced the apparent rate of ^{13}C-pyruvate to ^{13}C-lactate conversion and stressed out that the rate of metabolism of hyperpolarized pyruvate does not reflect the activity of LDH, but rather the activity of the MCT transporters in a breast cancer population [58]. However as shown by Witney et al. in a murine lymphoma cell line, the control of metabolite flux is probably shared between the membrane transporter and LDH [14].

Application in liver cancer

The incidence of liver cancer is continuously increasing and is usually diagnosed at a late stage [59]. Thus a sensitive non-invasive marker of disease with regard to prognosis and treatment of response is warranted. Yen et al. developed a single voxel based MRS sequence that was able to measure T_2 relaxation times of hyperpolarized ^{13}C-metabolites in vivo. They demonstrated that hyperpolarized ^{13}C-alanine and ^{13}C-lactate level were elevated in a rat model of hepatocellular carcinoma compared to normal liver tissue [60]. This was confirmed by Darpolor et al. who demonstrated that the conversion of hyperpolarized ^{13}C-pyruvate to ^{13}C-alanine and ^{13}C-lactate was associated with elevation of the enzymes of LDH and alanine transaminase (ALT) [61]. This suggests that the elevated levels of hyperpolarized ^{13}C-lactate and ^{13}C-alanine in hepatocellelular carcimona can be dependable upon the up-regulation of LDH and ALT. Hu et al. used a switchable transgenic mouse model with overexpression of the proto-oncogene *MYC* in the liver, giving rise to tumors that have features of human hepatocellular carcinoma and hepatoblastoma. Interestingly, conversion of ^{13}C-pyruvate to ^{13}C-alanine was predominant in very early stages of pre-tumor tissue, prior to any observable morphologic or histological changes. The increase of hyperpolarized ^{13}C-alanine level highlights the potential of ^{13}C-alanine as an early biomarker in liver cancer [62]. Continuously, a pulse sequence methodology was implemented to improve spatial resolution (to as high as 0.034 cm^3) and achieve up to a factor of 7.53 in acceleration for 3D spectroscopic imaging in the same transgenic mouse model of liver cancer. In clinical applications, this new pulse sequence could be used to cover a larger field of view [63] and therefore MRS could visualize larger volumes of tumors in one sequence. Menzel et al. demonstrated that hyperpolarized ^{13}C-pyruvate correlated with ^{18}F-FDG-PET in a rat model with hepatocellular carcinoma in most of the animals. Intratumoral heterogeneities due to necrosis could be identified in the ^{13}C metabolic and ^{18}F-FDG images [64].

Applications in other cancers

The first study using hyperpolarized ^{13}C-pyruvate in cancer used P22 tumor tissue, a highly malignant rat sarcoma. It was demonstrated that all implanted tumors showed significantly higher lactate content than the normal tissues and indicated that non-invasive quantification of localized Warburg effect may be possible [65]. Renal cell carcinoma is a very heterogeneous cancer with varying aggressiveness and prognosis. Differentiation between malignant and benign small renal tumors is difficult with conventional imaging, like ultrasound, CT and PET [66]. Keshari et al. demonstrated that hyperpolarized MRS of ^{13}C-pyruvate to ^{13}C-lactate ratio could be used to distinguish normal renal cells from renal cell carcinoma. In addition, they used the technique to show that metastatic renal cell carcinoma had a significantly higher ^{13}C-lactate/^{13}C-pyruvate ratio compared to the cells derived from localized renal cell carcinoma and that the differences were mediated by the MCT4 transporter [67].

Conclusion and perspective

The use of hyperpolarized ^{13}C-pyruvate for characterizing tumor metabolism has been demonstrated pre-clinically in an array of cancers. Recently the application was also shown clinically in prostate cancer. The information obtained is overlapping with that of ^{18}F-FDG-PET and the question is therefore if there is a role for clinical routine use of ^{13}C-pyruvate in cancer. We have demonstrated, for the first time, the feasibility of a new imaging concept combining hyperpolarized ^{13}C-pyruvate MRSI and ^{18}F-FDG-PET imaging [68]. A concept we have named *hyperPET* [69]. In a canine cancer patient with a biopsy verified sarcoma we found clearly increased ^{13}C-lactate production, which also corresponded to high ^{18}F-FDG uptake on PET. This is in agreement with the fact that glycolysis and production of lactate are increased in tumor cells compared to normal cells [68], see **Figures 3** and **4**. To the degree that ^{13}C-

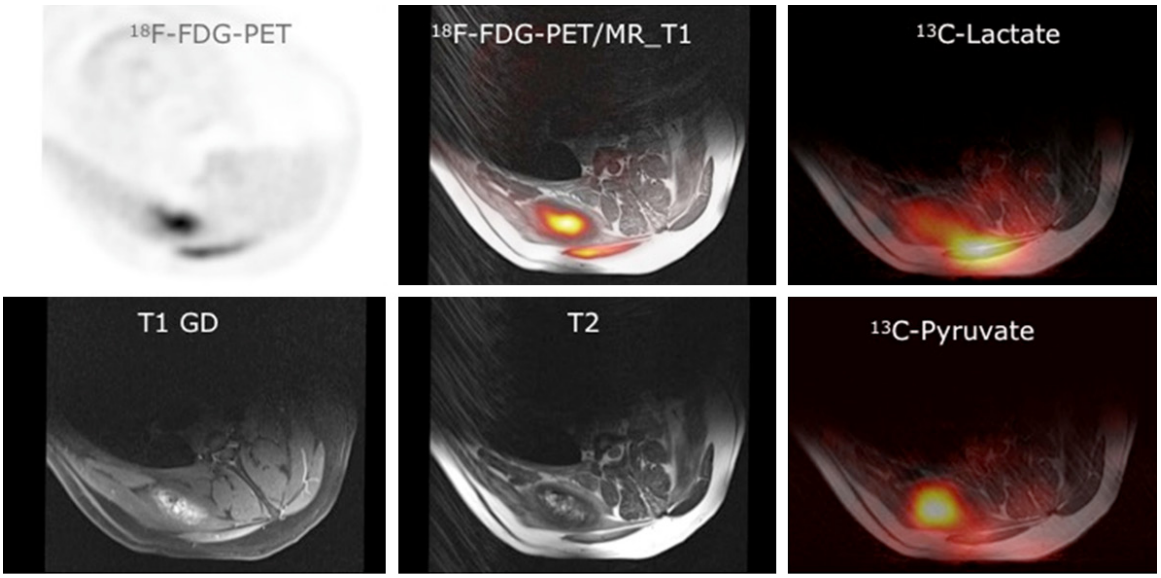

Figure 4. Showing Hyper PET images of a canine cancer patient with a sarcoma on the back. Demonstrating the agreement of ^{18}F-FDG and ^{13}C-lactate in the tumor region. Unpublished data.

pyruvate and ^{18}F-FDG-PET leads to similar information there is no doubt that ^{18}F-FDG is the method of choice: It is less costly, available in most hospitals, and renders whole body evaluation of metabolism. However, in some cancer types, e.g. prostate cancer ^{18}F-FDG-PET is not useful and here ^{13}C-pyruvate may represent an attractive alternative. Also in children, the concern of radiation burden could make ^{13}C-pyruvate the method of choice. With the emergence of hybrid PET/MR systems it is possible to conjoin ^{18}F-FDG-PET and ^{13}C-pyruvate MRS, which may be of increased value. With regard to early response monitoring in cancer treatment, the possibility exist that ^{13}C-pyruvate can detect such effect earlier and with higher sensitivity than other methods. Also this can only be answered through comparative PET and MR studies.

Address correspondence to: Dr. Andreas Kjaer, Department of Clinical Physiology, Nuclear Medicine & PET, KF-4012, Rigshospitalet, National University Hospital, Blegdamsvej 9, DK-2100 Copenhagen, Denmark. E-mail: akjaer@sund.ku.dk

References

[1] Gambhir SS. Molecular imaging of cancer with positron emission tomography. Nat Rev Cancer 2002; 2: 683-93.

[2] Adams MC, Turkington TG, Wilson JM, Wong TZ. A Systematic Review of the Factors Affecting Accuracy of SUV Measurements. AJR 2010; 195: 310-20.

[3] Patterson DM, Padhani AR, Collins DJ. Technology Insight: water diffusion MRI-a potential new biomarker of response to cancer therapy. Nat Clin Prac Oncol 2008; 5: 220-33.

[4] Kurhanewicz J, Swanson MG, Nelson SJ, Vigneron DB. Combined magnetic resonance imaging and spectroscopic imaging approach to molecular imaging of prostate cancer. J Magn Reson Imaging 2002; 16: 451 63.

[5] McKnight TR, Bussche von dem MH, Vigneron DB, Lu Y, Berger MS, McDermott MW, Dillon WP, Graves EE, Pirzkall A, Nelson SJ. Histopathological validation of a three-dimensional magnetic resonance spectroscopy index as a predictor of tumor presence. J Neurosurg 2002; 97: 794-802.

[6] Gujar SK, Maheshwari S, Bjorkman-Burtscher I, Sundgren PC. Magnetic resonance spectroscopy. Journal of Neuroophtalmology 2005; 25: 217-26.

[7] Shah N, Sattar A, Benanti M, Hollander S, Cheuck L. Magnetic resonance spectroscopy as an imaging tool for cancer: a review of the literature. J Am Osteopath Assoc 2006; 106: 23-7.

[8] Brindle K. Watching tumours gasp and die with MRI: the promise of hyperpolarised 13C MR spectroscopic imaging. Br J Radiol 2012; 85: 697-708.

[9] Kurhanewicz J, Vigneron DB, Brindle K, Chekmenev EY, Comment A, Cunningham CH, Deberardinis RJ, Green GG, Leach MO, Rajan SS, Rizi RR, Ross BD, Warren WS, Malloy CR. Analysis of cancer metabolism by imaging hyperpolarized nuclei: prospects for translation to clinical research. Neoplasia 2011; 13: 81-97.

[10] M Iler HE, Chen XJ, Saam B, Hagspiel KD, Johnson GA, Altes TA, de Lange EE, Kauczor HU. MRI of the lungs using hyperpolarized noble gases. Magn Reson Med 2002; 47: 1029-51.
[11] Natterer J, Bargon J. Parahydrogen induced polarization. Progr Nucl Magn Res Spectroscopy 1997; 31: 293–315.
[12] Witney TH, Brindle KM. Imaging tumour cell metabolism using hyperpolarized 13C magnetic resonance spectroscopy. Biochem Soc Trans 2010; 38: 1220-4.
[13] Ardenkjaer-Larsen JH, Fridlund B, Gram A, Hansson G, Hansson L, Lerche MH, Servin R, Thaning M, Golman K. Increase in signal-to-noise ratio of > 10,000 times in liquid-state NMR. Proc Natl Acad Sci U S A 2003; 100: 10158-63.
[14] Witney TH, Kettunen MI, Brindle KM. Kinetic modeling of hyperpolarized 13C label exchange between pyruvate and lactate in tumor cells. J Biol Chem 2011; 286: 24572-80.
[15] Jóhannesson H, Macholl S, Ardenkjaer-Larsen JH. Dynamic nuclear polarization of [1-13 C] pyruvic acid at 4.6 tesla. J Magn Reson 2009; 197: 167-75.
[16] Brindle KM, Bohndiek SE, Gallagher FA, Kettunen MI. Tumor imaging using hyperpolarized 13C magnetic resonance spectroscopy. Magn. Reson Med 2011; 66: 505-19.
[17] Ardenkjaer-Larsen JH, Jóhannesson H, Petersson JS, Wolber J. Hyperpolarized Molecules in Solution. In: In vivo NMR imaging : methods and protocols. Totowa, NJ: Humana Press; 2011. pages 205-26.
[18] Vander Heiden MG, Cantley LC, Thompson CB. Understanding the Warburg Effect: The Metabolic Requirements of Cell Proliferation. Science 2009; 324: 1029-33.
[19] Eisenhauer EA, Therasse P, Bogaerts J, Schwartz LH, Sargent D, Ford R, et al. New response evaluation criteria in solid tumours: Revised RECIST guideline (version 1.1). Pract Radiat Oncol 2014; 45: 240-6.
[20] Wahl RL, Jacene H, Kasamon Y, Lodge MA. From RECIST to PERCIST: Evolving Considerations for PET Response Criteria in Solid Tumors. J Nucl Med 2009; 50: 122S-150S.
[21] Kelly WK, Richon VM, O'Connor O, Curley T, MacGregor-Curtelli B, Tong W, Klang M, Schwartz L, Richardson S, Rosa E, Drobnjak M, Cordon-Cordo C, Chiao JH, Rifkind R, Marks PA, Scher H. Phase I clinical trial of histone deacetylase inhibitor: suberoylanilide hydroxamic acid administered intravenously. Clin Cancer Res 2003; 9: 3578-88.
[22] Song SY, Kim JH, Ryu JS, Lee GH, Kim SB, Park SI, Song HY, Cho KJ, Ahn SD, Lee SW, Shin SS, Choi EK. FDG-PET in the prediction of pathologic response after neoadjuvant chemoradiotherapy in locally advanced, resectable esophageal cancer. Int J Radiat Oncol Biol Phys 2005; 63: 1053-9.
[23] Hara T, Kosaka N, Kishi H. PET imaging of prostate cancer using carbon-11-choline. J Nucl Med 1998; 39: 990-5.
[24] Heiss WD, Raab P, Lanfermann H. Multimodality Assessment of Brain Tumors and Tumor Recurrence. J Nucl Med 2011; 52: 1585-600.
[25] Zhuang H, Pourdehnad M, Lambright ES, Yamamoto AJ, Lanuti M, Li P, Mozley PD, Rossman MD, Albelda SM, Alavi A. Dual Time Point 18F-FDG PET Imaging for Differentiating Malignant from Inflammatory Processes. J Nucl Med 2001; 42: 1412-7.
[26] Spaepen K, Stroobants S, Dupont P, Bormans G, Balzarini J, Verhoef G, Mortelmans L, Vandenberghe P, De Wolf-Peeters C. [18F]FDG PET monitoring of tumour response to chemotherapy: does [18F]FDG uptake correlate with the viable tumour cell fraction? Eur J Nucl Med Mol Imaging 2003; 30: 682-8.
[27] Evelhoch J, Garwood M, Vigneron D, Knopp M, Sullivan D, Menkens A, Clarke L, Liu G. Expanding the Use of Magnetic Resonance in the Assessment of Tumor Response to Therapy: Workshop Report. Cancer Res 2005; 65: 7041-4.
[28] Richon VM. Cancer biology: mechanism of antitumour action of vorinostat (suberoylanilide hydroxamic acid), a novel histone deacetylase inhibitor. Br J Cancer 2006; 95: S2-S6.
[29] Wei L, Hong S, Yoon Y, Hwang SN, Park JC, Zhang Z, Olson JJ, Hu XP, Shim H. Early prediction of response to Vorinostat in an orthotopic rat glioma model. NMR Biomed. 2012; 25: 1104-11.
[30] Day SE, Kettunen MI, Gallagher FA, Hu DE, Lerche M, Wolber J, Golman K, Ardenkjaer-Larsen JH, Brindle KM. Detecting tumor response to treatment using hyperpolarized 13C magnetic resonance imaging and spectroscopy. Nat Med 2007; 13: 1382-7.
[31] Witney TH, Kettunen MI, Day SE, Hu DE, Neves AA, Gallagher FA, Fulton SM, Brindle KM. A comparison between radiolabeled fluorodeoxyglucose uptake and hyperpolarized (13)C-labeled pyruvate utilization as methods for detecting tumor response to treatment. Neoplasia 2009; 11: 574-82.
[32] Witney TH, Kettunen MI, Hu DE, Gallagher FA, Bohndiek SE, Napolitano R, Brindle KM. Detecting treatment response in a model of human breast adenocarcinoma using hyperpolarised [1-13C]pyruvate and [1,4-13C$_2$]fumarate. Br J Cancer 2010; 103: 1400–6.
[33] Liu P, Cheng H, Roberts TM, Zhao JJ. Targeting the phosphoinositide3-kinase pathway in cancer. Nat Rev Cancer 2009; 8: 627-44.

[34] Howes AL, Chiang GG, Lang ES, Ho CB, Powis G, Vuori K, Abraham RT. The phosphatidylinositol 3-kinase inhibitor, PX-866, is a potent inhibitor of cancer cell motility and growth in three-dimensional cultures. Mol Cancer Ther 2007; 6: 2505-14.

[35] Ward CS, Venkatesh HS, Chaumeil MM, Brandes AH, Vancriekinge M, Dafni H, Sukumar S, Nelson SJ, Vigneron DB, Kurhanewicz J, James CD, Haas-Kogan DA, Ronen SM. Noninvasive detection of target modulation following phosphatidylinositol 3-kinase inhibition using hyperpolarized 13C magnetic resonance spectroscopy. Cancer Res 2010; 70: 1296-305.

[36] Chaumeil MM, Ozawa T, Park I, Scott K, James CD, Nelson SJ, Ronen SM. Hyperpolarized 13C MR spectroscopic imaging can be used to monitor Everolimus treatment in vivo in an orthotopic rodent model of glioblastoma. Neuroimage 2012; 59: 193-201.

[37] Park I, Bok R, Ozawa T, Phillips JJ, James CD, Vigneron DB, Ronen SM, Nelson SJ. Detection of early response to temozolomide treatment in brain tumors using hyperpolarized 13C MR metabolic imaging. J Magn Reson Imaging 2011; 33: 1284-90.

[38] Capdeville R, Buchdunger E, Zimmermann J, Matter A. Glivec (STI571, imatinib), a rationally developed, targeted anticancer drug. Nat Rev Drug Disc 2002; 1: 493-502.

[39] Dafni H, Larson PE, Hu S, Yoshihara HA, Ward CS, Venkatesh HS, Wang C, Zhang X, Vigneron DB, Ronen SM. Hyperpolarized 13C Spectroscopic Imaging Informs on Hypoxia-Inducible Factor-1 and Myc Activity Downstream of Platelet-Derived Growth Factor Receptor. Cancer Res 2010; 70: 7400-10.

[40] Tozer GM, Kanthou C, Baguley BC. Disrupting tumour blood vessels. Nat Rev Cancer 2005; 5: 423-35.

[41] Bohndiek SE, Kettunen MI, Hu DE, Witney TH, Kennedy BW, Gallagher FA, Brindle KM. Detection of Tumor Response to a Vascular Disrupting Agent by Hyperpolarized 13C Magnetic Resonance Spectroscopy. Mol Cancer Ther 2010; 9: 3278-88.

[42] Bohndiek SE, Kettunen MI, Hu DE, Brindle KM. Hyperpolarized (13)C spectroscopy detects early changes in tumor vasculature and metabolism after VEGF neutralization. Cancer Res 2012; 72: 854-64.

[43] Chen AP, Bok RA, Zhang V, Xu D, Veeraraghavan S, Hurd RE, et al. Serial hyperpolarized 13C 3D-MRSI following therapy in a mouse model of prostate cancer. Proc Intl Soc Mag Reson Med 2008; 16: 888.

[44] Day SE, Kettunen MI, Cherukuri MK, Mitchell JB, Lizak MJ, Morris HD, Matsumoto S, Koretsky AP, Brindle KM. Detecting response of rat C6 glioma tumors to radiotherapy using hyperpolarized [1- 13C]pyruvate and 13C magnetic resonance spectroscopic imaging. Magn Reson Med 2011; 65: 557-63.

[45] Macheda ML, Rogers S, Best JD. Molecular and cellular regulation of glucose transporter (GLUT) proteins in cancer. J Cell Physiol 2004; 202: 654-62.

[46] Lagerwaard F, Levendag P, Nowak P, Eijkenboom WH, Hanssens PJ, Schmitz PM. Identification of prognostic factors in patients with brain metastases: a review of 1292 patients. Int J Radiation Oncol Biol Phys 1999; 43: 795-803.

[47] García-Martín ML, Hérigault G, Rémy C, Farion R, Ballesteros P, Coles JA, Cerdán S, Ziegler A. Mapping Extracellular pH in rat Brain Gliomas in vivo by H Magnetic Resonance Spectroscopic Imaging: Comparison with maps of metabolites. Cancer Res 2001; 61: 6524-31.

[48] Saraswathy S, Crawford FW, Lamborn KR, Pirzkall A, Chang S, Cha S, Nelson SJ. Evaluation of MR markers that predict survival in patients with newly diagnosed GBM prior to adjuvant therapy. J Neurooncol 2009; 91: 69-81.

[49] Park I, Larson PE, Zierhut ML, Hu S, Bok R, Ozawa T, Kurhanewicz J, Vigneron DB, Vandenberg SR, James CD, Nelson SJ. Hyperpolarized 13C magnetic resonance metabolic imaging: application to brain tumors. Neuro Oncol 2010; 12: 133-44.

[50] Damber JE, Aus G. Prostate cancer. The Lancet 2008; 371: 1710-21.

[51] Hughes C. Molecular pathology of prostate cancer. J Clin Pathol 2005; 58: 673-84.

[52] Kaplan-Lefko PJ, Chen TM, Ittmann MM, Barrios RJ, Ayala GE, Huss WJ, Maddison LA, Foster BA, Greenberg NM. Pathobiology of autochthonous prostate cancer in a pre-clinical transgenic mouse model. Prostate 2003; 55: 219-37.

[53] Chen AP, Albers MJ, Cunningham CH, Kohler SJ, Yen YF, Hurd RE, Tropp J, Bok R, Pauly JM, Nelson SJ, Kurhanewicz J, Vigneron DB. Hyperpolarized C-13 spectroscopic imaging of the TRAMP mouse at 3T-Initial experience. Magn Reson Med 2007; 58: 1099-106.

[54] Albers MJ, Bok R, Chen AP, Cunningham CH, Zierhut ML, Zhang VY, Kohler SJ, Tropp J, Hurd RE, Yen YF, Nelson SJ, Vigneron DB, Kurhanewicz J. Hyperpolarized 13C Lactate, Pyruvate, and Alanine: Noninvasive Biomarkers for Prostate Cancer Detection and Grading. Cancer Res 2008; 68: 8607-15.

[55] Lupo JM, Chen AP, Zierhut ML, Bok RA, Cunningham CH, Kurhanewicz J, Vigneron DB, Nelson SJ. Analysis of hyperpolarized dynamic 13C lactate imaging in a transgenic mouse model of prostate cancer. Magn Reson Med 2010; 28: 153-62.

[56] Nelson SJ, Vigneron DB, Kurhanewicz J, Chen AP, Bok RA, Hurd RE. DNP-Hyperpolarized 13C Magnetic Resonance Metabolic Imaging for Cancer Applications. Appl Magn Reson 2008; 34: 533-44.

[57] Nelson SJ, Kurhanewicz J, Vigneron DB, Larson PE, Harzstark AL, Ferrone M, van Criekinge M, Chang JW, Bok R, Park I, Reed G, Carvajal L, Small EJ, Munster P, Weinberg VK, Ardenkjaer-Larsen JH, Chen AP, Hurd RE, Odegardstuen LI, Robb FJ, Tropp J, Murray JA. Metabolic imaging of patients with prostate cancer using hyperpolarized [1-^{13}C]pyruvate. Sci Transl Med 2013; 5: 198ra108.

[58] Harris T, Eliyahu G, Frydman L, Degani H. Kinetics of hyperpolarized 13C1-pyruvate transport and metabolism in living human breast cancer cells. Proc Natl Acad Sci U S A 2009; 106: 18131-6.

[59] El-Serag HB, Rudolph KL. Hepatocellular Carcinoma: Epidemiology and Molecular Carcinogenesis. Gastroenterology 2007; 132: 2557-76.

[60] Yen YF, Le Roux P, Mayer D, King R, Spielman D, Tropp J, Butts Pauly K, Pfefferbaum A, Vasanawala S, Hurd R. T(2) relaxation times of (13)C metabolites in a rat hepatocellular carcinoma model measured in vivo using (13)C-MRS of hyperpolarized [1-(13)C]pyruvate. NMR Biomed 2010; 23: 414-23.

[61] Darpolor MM, Yen YF, Chua MS, Xing L, Clarke-Katzenberg RH, Shi W, Mayer D, Josan S, Hurd RE, Pfefferbaum A, Senadheera L, So S, Hofmann LV, Glazer GM, Spielman DM. In vivo MRSI of hyperpolarized [1-13C]pyruvate metabolism in rat hepatocellular carcinoma. NMR Biomed 2011; 24: 506-13.

[62] Hu S, Balakrishnan A, Bok RA, Anderton B, Larson PE, Nelson SJ, Kurhanewicz J, Vigneron DB, Goga A. 13C-pyruvate imaging reveals alterations in glycolysis that precede c-Myc-induced tumor formation and regression. Cell Metab 2011; 14: 131-42.

[63] Hu S, Lustig M, Balakrishnan A, Larson PE, Bok R, Kurhanewicz J, Nelson SJ, Goga A, Pauly JM, Vigneron DB. 3D compressed sensing for highly accelerated hyperpolarized 13C MRSI with in vivo applications to transgenic mouse models of cancer. Magn. Reson Med 2010; 63: 312-21.

[64] Menzel MI, Farrell EV, Janich MA, Khegai O, Wiesinger F, Nekolla S, Otto AM, Haase A, Schulte RF, Schwaiger M. Multimodal Assessment of In Vivo Metabolism with Hyperpolarized [1-13C] MR Spectroscopy and 18F-FDG PET Imaging in Hepatocellular Carcinoma Tumor-Bearing Rats. J Nucl Med 2013; 54: 1113-9.

[65] Golman K, Zandt RI, Lerche M, Pehrson R, Ardenkjaer-Larsen JH. Metabolic Imaging by Hyperpolarized 13C Magnetic Resonance Imaging for In vivo Tumor Diagnosis. Cancer Res 2006; 66: 10855-60.

[66] Bolton DM, Wong P, Lawrentschuk N. Renal cell carcinoma: imaging and therapy. Curr Opin Urol 2007; 17: 337-40.

[67] Keshari KR, Sriram R, Koelsch BL, Van Criekinge M, Wilson DM, Kurhanewicz J, Wang ZJ. Hyperpolarized 13C-pyruvate magnetic resonance reveals rapid lactate export in metastatic renal cell carcinomas. Cancer Res 2013; 73: 529-38.

[68] Gutte H, Hansen AE, Henriksen ST, Johannesen HH, Ardenkjaer-Larsen J, Vignaud A, Hansen AE, Børresen B, Klausen TL, Wittekind AM, Gillings N, Kristensen AT, Clemmensen A, Højgaard L, Kjær A. Simultaneous hyperpolarized (13)C-pyruvate MRI and (18)F-FDG-PET in cancer (hyperPET): feasibility of a new imaging concept using a clinical PET/MRI scanner. Am J Nucl Med Mol Imaging 2014; 5: 38-45.

[69] Gutte H, Hansen AE, Larsen M, Rahbek S, Henriksen S, Johannesen H, Ardenkjær-Larsen J, Kristensen A, Højgaard L, Kjær A. Simultaneous hyperpolarized 13C-pyruvate MRI and 18F-FDG-PET (hyperPET) in 10 canine cancer patients. J Nucl Med 2015; [Epub ahead of print].

[70] Henderson W, McIndoe JS. Mass Spectrometry of Inorganic, Coordination and Organometallic Compounds. 1st ed. West Sussex, England: Wiley; 2005.